crystals

MDPI

Article

Synthetic Conditions for Obtaining Different Types of Amine-Holding Silica Particles and Their Sorption Behavior

Inna Melnyk [1,2,*], Veronika Tomina [2] and Nataliya Stolyarchuk [2]

[1] Department of Physical and Physico-Chemical Methods of Mineral Processing, Institute of Geotechnics SAS, 45, Watsonova, 04001 Košice, Slovakia
[2] Department of Chemisorption and Hybrid Materials, Chuiko Institute of Surface Chemistry NASU, 17, Generala Naumova, 03164 Kyiv, Ukraine
* Correspondence: melnyk@saske.sk; Tel.: +421-55-7922612

Abstract: The Stöber version of a sol-gel method of co-condensation of two alkoxysilanes (structuring tetraethoxysilane (TEOS) and functionalising N-containing silane) in an ammonia medium was used for the one-pot synthesis of spherical silica particles with $\equiv Si(CH_2)_3NH_2$, $\equiv Si(CH_2)_3NH(CH_2)_2NH_2$, and $\equiv[Si(CH_2)_3NH]_2$ functional groups with available groups content of 1.3–2.3 mmol/g. The materials were researched by a range of methods, including SEM, TEM, IR spectroscopy, ^{13}C, and ^{29}Si solid-state NMR spectroscopy, acid-base titration, and thermal analysis to identify the peculiarities of the morphology, functional groups content, composition, and thermal resistance of the surface layers in the synthesised samples. The type of N-containing silane was shown to affect the structure and properties of the synthesised spherical particles. The silane with the simplest, 3-aminopropyl, functional group caused the formation of nonporous material composed of large 600–800 nm spherical microparticles. Meanwhile, the complication of functional groups enhanced the emergence of small 15 nm primary particles and the origination of porosity, generated by the slits between particles and particle agglomerates. Thereafter, the sorption properties of the synthesised hybrid materials for nickel(II) and copper(II)ions, and bovine serum albumin (BSA) were also found to be dependent on the structure of the materials and the type of incorporated functional group. The maximal static sorption capacity values towards the targeted adsorbates were shown by the samples with 3-aminopropyl groups (1.27 mmol Ni/g), diamine groups (1.09 mmol Cu/g), and secondary amine groups (204.6 mg BSA/g). The conducted research opens up the prospects of directed one-pot synthesis of amino-functionalised hybrid organosilica materials for different applications.

Keywords: sol-gel technique; one-pot synthesis; 3-aminopropyl groups; ethylenediamine groups; secondary amine groups; Cu(II) ions sorption; Ni(II) ions sorption; bovine serum albumin sorption

check for updates

Citation: Melnyk, I.; Tomina, V.; Stolyarchuk, N. Synthetic Conditions for Obtaining Different Types of Amine-Holding Silica Particles and Their Sorption Behavior. *Crystals* **2023**, *13*, 190. https://doi.org/10.3390/cryst13020190

Academic Editors: Aleksej Zarkov, Aivaras Kareiva and Loreta Tamasauskaite-Tamasiunaite

Received: 30 December 2022
Revised: 17 January 2023
Accepted: 18 January 2023
Published: 21 January 2023

1. Introduction

The influence of anthropogenic factors on environmental pollution has aggravated recently. Heavy metals that are widely used in various industries form a special group of pollutants [1]. Heavy metal ions are usually distributed in the environment by means of water [2]. Therefore, their removal from water is an urgent problem that constantly causes concern [3]. Respecting sorption technologies, the search for approaches to synthesise novel materials with a well-developed porous structure (ensuring good kinetic characteristics) and a high content of available functional groups is worthy of attention.

Silica-based materials can be used for catalysis and environmental applications [4]. However, the efficiency of pure silica sorbents is relatively low [5]. To improve the sorption properties of these materials, oxygen-, nitrogen-, or sulfur-containing functional groups are incorporated into them [6]. Recently, silicas functionalised with amino groups have been of considerable interest, because their surface layer allows binding ions of such metals as copper and nickel into stable complex compounds [7,8]. Nitrogen-containing polysiloxane

sorbents have been well-studied, described in detail in [9,10], and even produced as commercial materials [11,12].

It should be mentioned that sorption materials formed by spherical particles are more effective for sorption processes from a technological point of view. Such materials are characterised by greater availability of complex-forming functional groups for interaction with metal ions, which improves the process of extraction of metal ions from their aqueous solutions. Sorption materials in the form of spherical particles can be prepared using the Stöber version of sol-gel synthesis [13]. Spherical silica particles with amino groups have recently been very popular as carriers for various applications, such as drug delivery [14], chemotherapy [15], biomedicine [16], antibacterial therapy [17], liquid chromatography [18], catalysis [19]; as fillers for the flame retardants [20]; as sorbents of organic molecules [21,22], gasses [23,24], and metal ions [25–27]. Therefore, their economically feasible production is an urgent task. In many cases in the above-mentioned references, surface modification was used to attach amino groups to the silica surface, while a template method was applied to create mesoporous materials. Functionalising alkoxysilanes of different compositions can be used to affix different types of nitrogen-containing groups onto the surface of the materials. Previously, we described a one-step synthesis of aminosilica particles [28] and the possibility of influencing their size and surface chemistry [29]. Moreover, for the certain tasks, silanes with diamine groups [30,31] and bridged silanes with amino groups [32,33] are increasingly used, so the research data will be of practical interest to the scientists in this area. The main idea of this work is to use the Stöber method for the one-component system (TEOS) and apply it to the two-component system, where the second component is a silane with amino groups of different structure. In this study, it is proposed to obtain in one step silica spheres with 3-aminopropyl groups, diamine groups (which increases the number of heteroatoms on the surface), as well as to synthesise materials with bridging silanes containing a secondary amino group and affecting the porosity of the obtained materials. It was shown that the suggested method of synthesis promotes the fixation of a large number of amino-containing groups and they are available for interactions with metal cations and protein molecules on the example of bovine serum albumin.

2. Materials and Methods

2.1. Reagents

The following substances were used to prepare the samples: tetraethoxysilane, $Si(OC_2H_5)_4$ (TEOS, 98%, Aldrich, St.Louis, MO, USA); 3-aminopropyltriethoxysilane, $C_9H_{23}NO_3Si$ (APTES, 98%, Fluka); N-[3-(trimethoxysilyl)propyl]ethylenediamine, $C_8H_{22}N_2O_3Si$ (TMPED, 97%, Aldrich, USA); bis [3-(trimethoxysilyl)propyl]amine, $[(CH_3O)_3Si(CH_2)_3]_2NH$ (BTMPA, 95%, ABCR); ethanol (96%, Ukrspirt); ammonia solution, 25% (NH_4OH, p.a., Macrochem, Ukraine).

Reagents used for acid-base titration and sorption: $Cu(NO_3)_2 \cdot 3H_2O$ (Merck); $Ni(NO_3)_2 \cdot 3H_2O$ (Macrochem, Ukraine); bovine serum albumin (BSA, for biochemistry, protease free, Acros organics); buffer aqueous solution (phosphate buffered saline tablets, Fisher BioReagents, pH = 7.4); solutions of 0.1 M HNO_3, 0.1 M NaOH, and 0.1 M HCl prepared from fixanal concentrates; 0.1 M $NaNO_3$ solution prepared from $NaNO_3$ salt (chem.pure, Macrochem, Ukraine), methyl orange (1% solution prepared from methyl orange powder, chem.pure, Macrochem, Ukraine).

2.2. Synthesis of Silica-Based Particles with Amino Groups in the Surface Layer

For the synthesis of TEOS/APTES, TA (and TEOS/TMPED, TEDA) samples, 100 cm^3 (70 cm^3) of ethanol, 21.7 cm^3 of NH_4OH and 14 cm^3 of distilled water were mixed in a glass at a constant stirring with a magnetic stirrer. In a few minutes, 2 cm^3 (0.0083 mol) of APTES (1.9 cm^3 (0.0085 mol) of TMPED) were added, followed by 6 cm^3 (0.0263 mol) of TEOS. The precipitation started in 2 min (after that for TEDA, another 30 cm^3 of ethanol were added).

For the synthesis of TEOS/BTMPA, TBA sample, 30 cm^3 of ethanol, 21.7 cm^3 of NH_4OH and 14 cm^3 of distilled water were mixed in a glass at a constant stirring with a magnetic stirrer. Then, 2.8 cm^3 (0.0081 mol) of BTMPA in 40 cm^3 of ethanol were added to

the reaction, followed by 6 cm^3 (0.0263 mol) of TEOS. In 2 min, the precipitation started, and when in several more minutes the precipitate turned curd-like, another 30 cm^3 of ethanol was added to the reaction.

In general, the molar ratio of TEOS/N-containing silane was ~3/1 (Table 1). The reactions continued for 1 h. The particles were separated from the solutions by centrifugation (10 min, 5000 rpm), and washed 3 times with ethanol. The samples were dried at 120 °C for 3 days.

Table 1. The content of functional groups in the studied samples and the value of the specific surface.

Sample Composition and Its Label	Molar Ratio TEOS/Amino-Silane	C_{groups} Theor., mmol/g	C_{groups} Titrat., mmol/g	C_{groups} Therm.an., mmol/g	S_{sp}, m^2/g
$SiO_2/{\equiv}Si(CH_2)_3NH_2$ (TA)	3/1	3.3	1.3	1.9	17
$SiO_2/{\equiv}Si(CH_2)_3NH(CH_2)_2NH_2$ (TEDA)	3/1	3.0	2.3	2.9	174
$SiO_2/[{\equiv}Si(CH_2)_3]_2NH$ (TBA)	3/1	2.6	2.0	2.1	179

2.3. Analysis Methods

The content of amine functional groups on the surface of the synthesised silica particles was determined by the method of acid-base back titration [34]. It is based on the determination of the number of protons absorbed by the amino group after holding the sorbent batch (0.1 g) in an excess of 0.1 M HCl solution (with periodic stirring) until equilibrium is established (72 h). The excess of hydrochloric acid was titrated with 0.1 M NaOH and methyl orange as an indicator.

Scanning electron microscopy (SEM) is widely used to study the morphology of sorbents and determine their particle sizes. The sample was mounted on the surface of the table with a pre-applied adhesive coating and sputtered with gold by the method of cathodic sputtering. The SEM images were collected with a scanning electron microscope JSM 6060 LA (Jeol, Tokyo, Japan) in the secondary electron mode at an accelerating voltage of 30 kV. The materials (previously deposited on a transparent carbon film on a copper substrate) were also analysed by transmission electron microscopy (TEM) using TEM/HRTEM (JEOL JEM 2010-Fx) at 200 kV and energy-dispersive X-ray spectroscopy (EDXS).

Nitrogen adsorption-desorption isotherms for all samples were collected using a Kelvin-1042 sorptometer. The samples were previously degassed in a helium stream at 110 °C for 1 h. The specific surface area (S_{sp}) was calculated according to BET [35] in the range of relative pressures 0.05–0.35.

Infrared (IR) reflectance spectra of the samples ground with KBr (FT-IR grade, Sigma-Aldrich) at 1/20 weight ratio were recorded on a Thermo Nicolet Nexus FTIR spectrometer using the "SMART Collector" diffuse reflectance attachment in the region of 4000–400 cm^{-1} at a resolution of 8 cm^{-1}.

The thermal analysis (differential thermal analysis (DTA), differential thermal gravimetry (DTG), and thermogravimetry (TG)) was performed on the MOM Q-1500 D (Paulik–Paulik–Erdey) derivatograph operating in the range of 20–1000 °C, with a heating rate of 10 °C·min^{-1}.

The ^{13}C and ^{29}Si MAS NMR experiments were conducted on a Bruker Avance II 400 spectrometer with 4 mm rotors (ZrO_2) spun at 10 kHz. ^{13}C NMR spectra were measured using $^{1}H \rightarrow {}^{13}C$ CP/MAS, ^{1}H decoupling during acquisition, a contact time of 3 ms, and 5 s of recycle delay. The number of scans was between 768 and 2300. ^{29}Si NMR spectra were recorded with 3 µs excitation pulses, a contact time of 2 ms, and 5 s of recycle delay. The number of scans was between 640 and 1024. ^{13}C and ^{29}Si chemical shifts are referenced towards 4,4-dimethyl-4-silapentane-1-sulfonic acid (DSS).

2.4. Adsorption Studies

The sorption of heavy metals nickel(II) and copper(II) was studied under static conditions. A batch of sorbent (0.05 g) was poured with 25 cm^3 of working solutions of metal

ions. The content of copper and nickel in the aqueous phase was determined by the atomic absorption method on a C-115-M1 spectrophotometer along the resonance line of 324.7 nm (for copper) and 232.0 nm in a depleted (oxidizing) flame of an acetylene/air mixture. The source of resonant radiation was the LS-2 spectral lamp. The detection limit for metals was 0.01 μg/cm^3.

To study the physical adsorption of bovine serum albumin (BSA) from aqueous solution on functionalised nanoparticles, there was used 1% BSA stock solution in phosphate saline buffer and its diluted solutions 0.1–1.0%. UV–Vis spectrophotometer Helios Gamma (Thermo Electron Corporation, Great Britain) was used to register absorption spectra of BSA in solution. Experimental conditions: m = 0.02 g, V (working volume of albumin solution) = 10 cm^3, the contact time of phases was 1.0 h, t = 36°C. The equilibrium concentration of albumin was determined spectrophotometrically at λ = 278 nm (the thickness of the cell = 1 cm) after removing the sorbent.

3. Results and Discussion

In the current research we synthesised three different types of particles via co-condensation of TEOS (as the main structuring agent) and divergent amino-containing silanes (as functionalising agents), as schematically depicted in Figure 1 and summarized in Table 1. The first sample (**TA**) is carrying the usual 3-aminopropyl groups incorporated with APTES. The second sample (**TEDA**) bears (propyl)ethylenediamine functional groups, i.e., it has lengthened aminoorganic fragments with larger number of nitrogen donor centres. Finally, the third sample (**TBA**) carries secondary amino groups introduced by means of a bissilane having an amino group in the structure of the bridge. The syntheses of sorption materials were carried out in the same conditions of a water-ethanol environment with a molar ratio of reacting components TEOS/functionalising alkoxysilane of 3/1. Ammonium hydroxide was used as a catalyst for the hydrolytic polycondensation reaction [13].

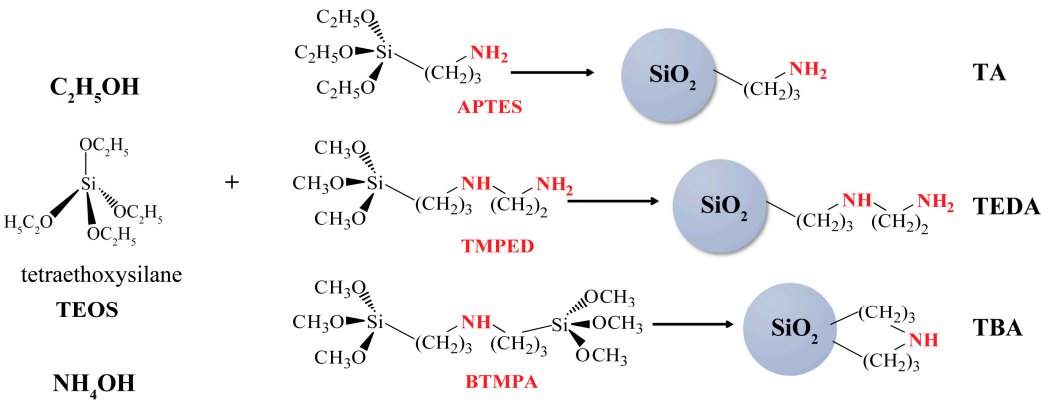

Figure 1. Synthesis of amino-containing spherical silica particles.

3.1. Morphology

The morphology and sizes of the synthesised particles were analysed with SEM microphotographs. In keeping with the SEM and TEM images of the **TA** sample presented in Figure 2, the material is formed by clearly visible spherical particles from 600 to 800 nm in size. Meanwhile, samples **TEDA** and **TBA** (Figure 2) are formed by 220–275 nm agglomerates and aggregates, whereas their primary particles are much smaller in size ~15 nm. That is, by the developed technique of synthesis, the emerging silica spheres with 3-aminopropyl groups are spherical microparticles with a size of 500–800 nm. In the same conditions of synthesis, the introduction of a larger functional group, as well as a group with a higher basicity, leads to the formation of much smaller-sized primary particles, which tend to agglomerate. Such a difference is explained by the rates of hydrolysis and condensation. The kinetics of hydrolysis of methoxy derivatives (functionalising methoxy silanes TMPED and BTMPA used in the synthesis of **TEDA** and **TBA** samples, respectively) is very fast, faster than that of ethoxy derivatives (functionalising ethoxy silanes APTES used in the

synthesis of **TA** sample). However, the rate of condensation decreases with the increase in the size of the organic group near the silicon atom [36]. Thus, slow hydrolysis and fast condensation of APTES in the case of **TA** sample result in the formation of large microspheres. Meanwhile, fast hydrolysis and slow condensation of TMPED and BTMPA, as well as electrosteric barriers prevent the primary particles from uniting into spherical secondary particles and facilitating dendromer formation [37], lead to the emergence of 15 nm particles of **TEDA** and **TBA** samples.

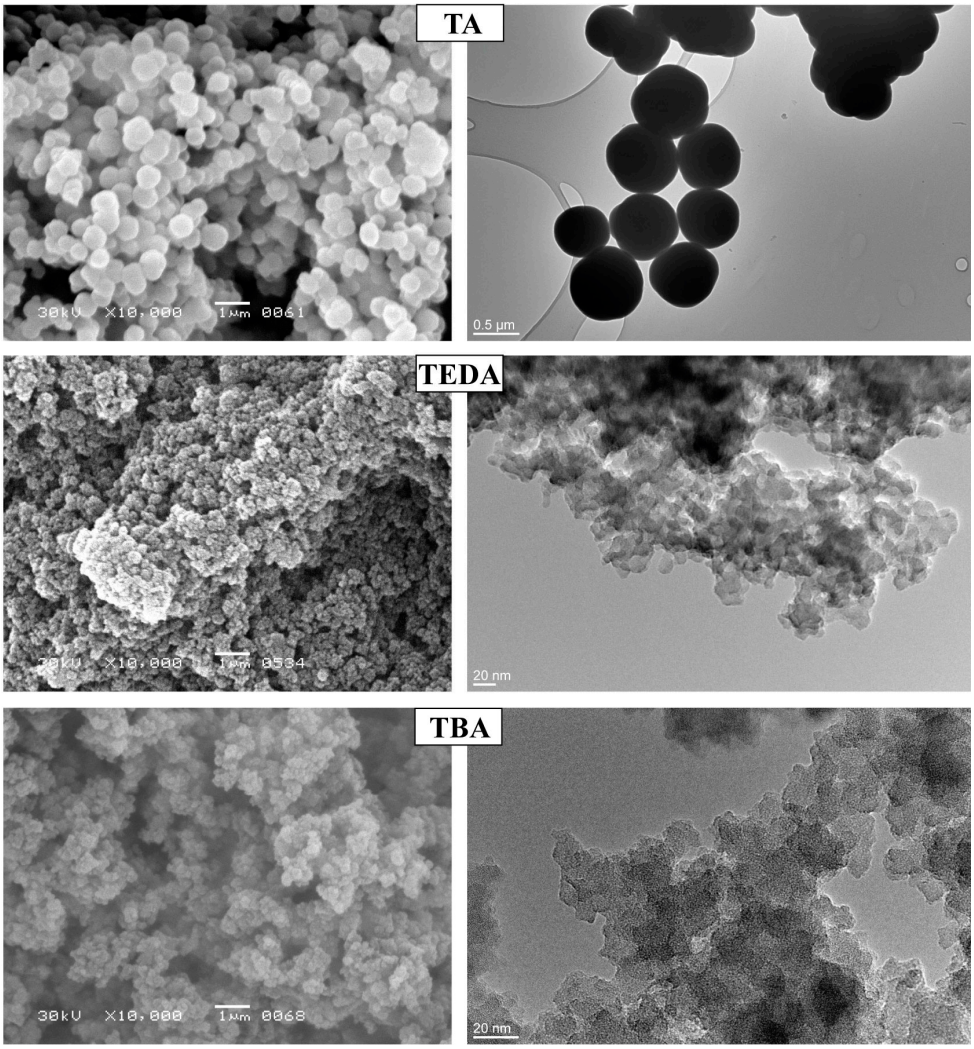

Figure 2. SEM (the **left** column) and TEM (the **right** column) images of the synthesised samples.

3.2. The Composition and Structure of the Obtained Samples

Table 1 shows the values of the specific surface area for silica-based samples, which were calculated from the isotherms of low-temperature nitrogen adsorption-desorption (Figure 3). These data correlate with TEM data and are related to the particle sizes. Observing the results of low-temperature nitrogen adsorption-desorption analysis, 3-aminopropyl-bearing **TA** is a non-porous sample with the value of the specific surface $S_{sp.}$ = 17 m^2/g (Table 1), which is consistent with its large particle sizes (about 600–800 nm). Meanwhile, **TEDA** material with ethylenediamine groups and **TBA** material with secondary amine groups, formed by much smaller primary particles, are characterised by specific surfaces of 174 and 179 m^2/g. Calculations based on the SCV/SCR method [38] have shown that most pores are formed by slits between particles and particle agglomerates, and belong to mesopores for the **TEDA** sample and meso- and macropores for the **TBA** sample (Figure S1, Table S1) (see Supplementary Materials).

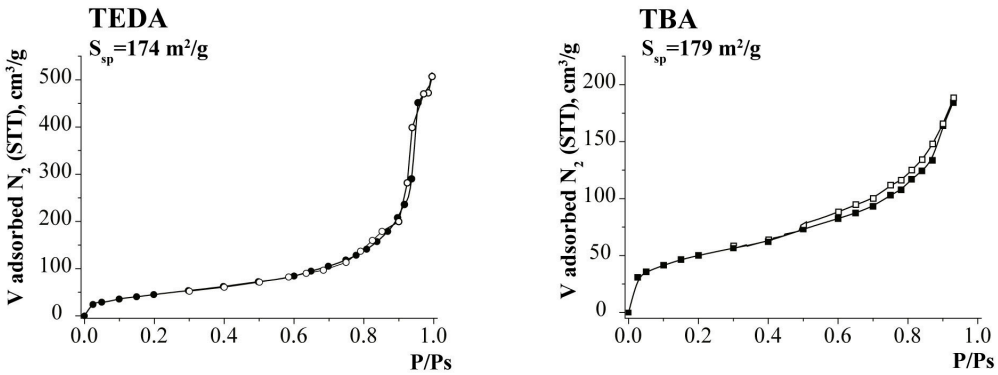

Figure 3. Low-temperature nitrogen adsorption-desorption isotherms for **TEDA** and **TBA** samples.

The IR spectra of the samples are illustrated in Figure 4. All of them contain an intense absorption band in the region of 1000–1200 cm^{-1} with a shoulder in the higher frequencies, which is characteristic of ν(Si-O-Si) stretches and indicates the formation of a network of polysiloxane bonds. A broad absorption band at 3300 cm^{-1} and a band of medium intensity at 1630–1640 cm^{-1} are caused by stretching and bending vibrations of water molecules adsorbed on the surface of the samples. However, there are absorption bands of amino groups in the same region [39] overlapping with water vibrations: two low-intensity absorption bands for **TA** and **TEDA** samples, and one weak band for **TBA** in the region of 3288–3366 cm^{-1} are related to $\nu_{s,as}$(NH) of the amino groups involved in the hydrogen bond. An additional band at ~1540 cm^{-1} refers to deformations $\delta(NH_2)$ of NH_2 groups [31], while a broad strong absorption band around ~800 cm^{-1} belongs to wagging and twisting vibrations of NH_2 (in **TA** and **TEDA**) and NH wagging (in **TBA**).

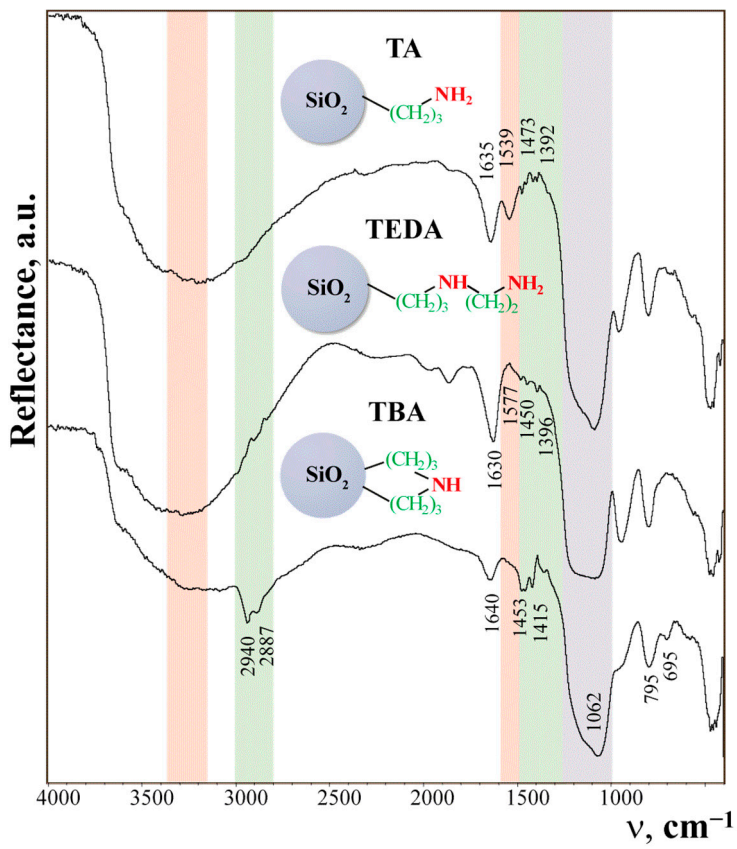

Figure 4. IR spectra of the synthesised samples.

Absorption bands in the region of 2850–2950 cm^{-1} belong to symmetric and asymmetric CH stretches of the aminopropyl radical, whereas a group of bands in the 1350–1480 cm^{-1} region correspond to bending vibrations of CH_2.

Summarizing the analysis of the IR spectra, the particles that were synthesised consist of a well-developed polysiloxane network with affixed targeted amine functional groups.

Furthermore, EDXS data (Figure S2) also confirm the existence of nitrogen-containing functional groups in the surface layers of the silica particles (for the **TA** sample, due to the small number of functional groups, signal N-K, apparently overlaps with oxygen signal).

The quantitative content of the organic component in the prepared samples was additionally assessed on the basis of thermal analysis data (Figure 5). Analysing thermoanalytical curves, all the samples lose weight when heated to 100 °C (**TA**—7.9%; **TEDA**—5.5%; **TBA**—12.2%), which can be associated with the removal of the remains of sorbed water, the evidence of which in the samples was also recorded by IR spectra. The **TEDA** and **TBA** samples have similar thermograms. For the **TEDA** sample, the exoeffect at 230 °C is more pronounced than for the **TBA** sample at 275 °C, and it is completely absent in the **TA** sample. The reason for such a difference may lie both in the porosity and in the more complex structure of the functional groups in **TEDA** and **TBA**, due to which the organic component burns out unevenly in several stages. The lack of endo effects above 200 °C in the DTG curve and the presence of exoeffects in the DTA curve of **TA** sample indicate processes of oxidation of organic groups, accompanied by the weight loss at a constant speed, due to the mutually compensating processes of formation and collapse of decomposition compounds [40]. Taking into account the weight loss for the combustion of the organic groups, the number of functional groups in the samples were calculated, and they agree with the titration data (Table 1). Following Table 1, amino groups content in the spherical silica microparticles **TA** is about 2 times less than in samples **TEDA** and **TBA**. Again, such a relatively high content of functional groups (**TEDA** and **TBA**) at the taken ratio of reacting components is more typical for xerogels with amino groups [41].

The ^{13}C NMR spectra (Figure 6, Table 2) of the synthesised samples confirm the presence of functional groups introduced during the synthesis, as well as the presence of residual ethoxy and methoxy groups [42,43]. These results correlate with the data of ^{29}Si NMR spectroscopy (Figure 6, Table 3). The presence of methoxy groups in the prepared samples demonstrates an incompleteness of hydrolysis of nitrogen-containing alkoxysilanes (TMPED or BTMPA) and, accordingly, explains the appearance of signals in ^{29}Si NMR spectra at ~57–58 ppm related to the T^2 structural units [32]. In addition, in the ^{29}Si NMR spectrum of the **TBA** sample (Figure 6), a signal at −50.5 ppm corresponding to the T^1 structural unit is observed (Table 3). The appearance of such a structural unit may be related to the nature of functionalising alkoxysilane (bissilane BTMPA), when the hydrolysis and polycondensation processes are hindered by the size of the bridging group. Such hindered hydrolysis and polycondensation of BTMPA may be one of the reasons for lower content of functional groups in **TBA** compared to **TEDA** sample (Table 1). However, as secondary amino groups of **TBA** are located within polysiloxane network, some of them may be both unavailable for titration and their burnout may be complicated. The presence in the ^{29}Si NMR spectra of **TA** of only Q^4 and Q^3 structural units indicates the completeness of hydrolysis in the TEOS/APTES system [44].

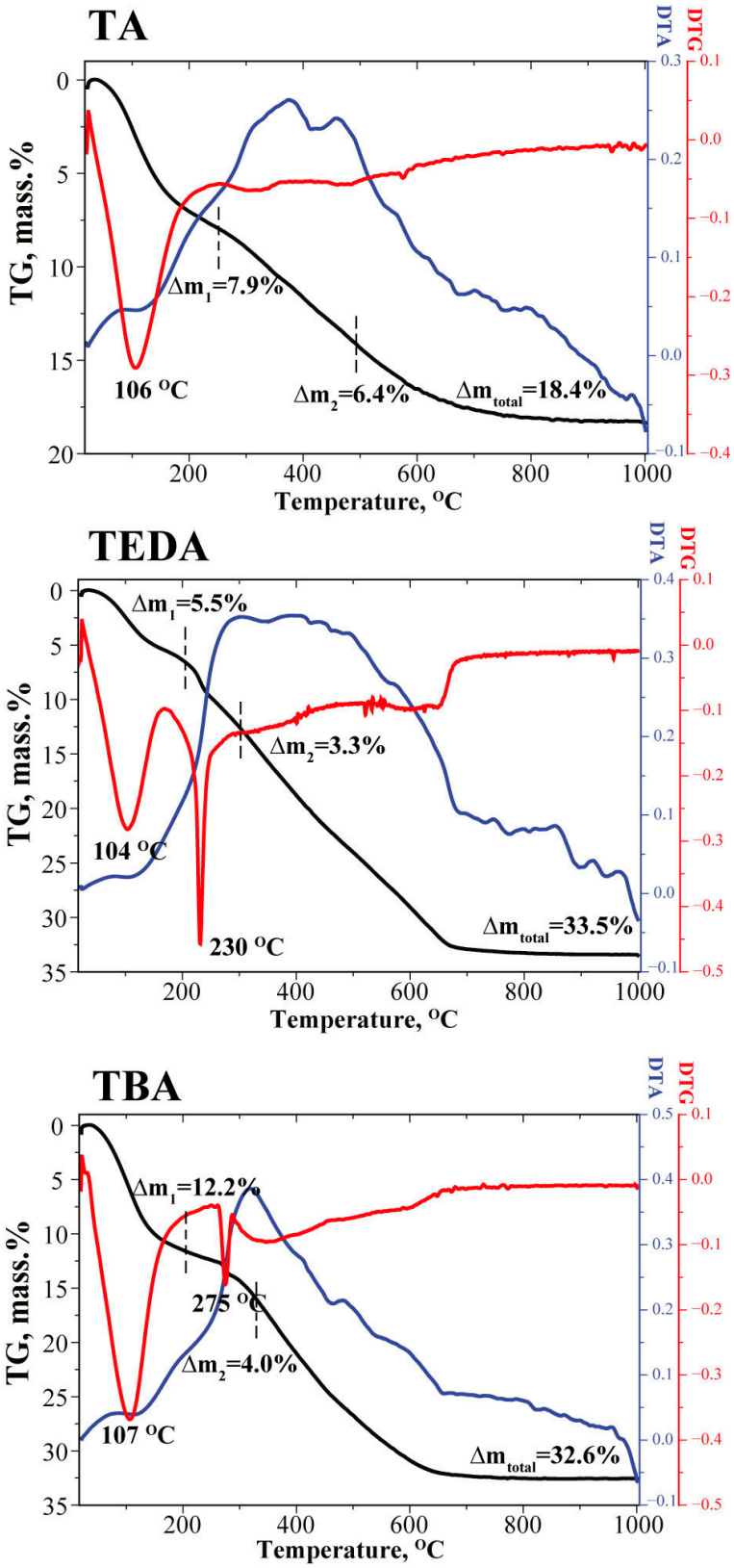

Figure 5. Thermoanalysis curves for the amino-containing samples.

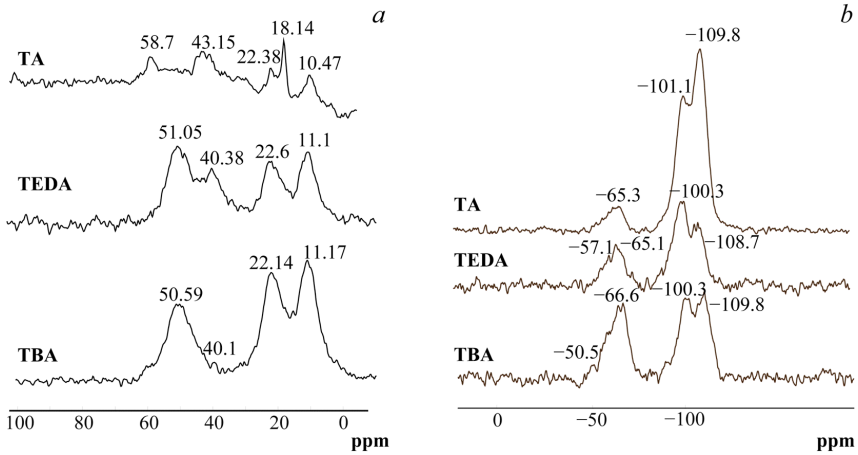

Figure 6. ^{13}C NMR spectra (**a**) and ^{29}Si NMR spectra (**b**) of synthesised samples.

Table 2. ^{13}C CP/MAS NMR spectroscopy data for samples with nitrogen-containing groups.

Peak Assignments	Chemical Shifts, ppm		
	TA	TEDA	TBA
≡Si-$\underline{C}H_2$-CH_2-CH_2- N	10.47	11.1	11.17
≡Si-O-$\underline{C}H_2$-CH_3	18.14	-	-
≡Si-CH_2-$\underline{C}H_2$-CH_2-N	22.38	22.6	22.14
≡Si-CH_2-CH_2-$\underline{C}H_2$-N	43.15	40.38	40.1
≡Si-O-$\underline{C}H_3$	-	51.05	50.59
≡Si-O-CH_2-$\underline{C}H_3$	58.7	-	-

Table 3. ^{29}Si CP/MAS NMR spectroscopy data for samples with nitrogen-containing groups.

Structural Units	Chemical Shifts, Ppm		
	TA	TEDA	TBA
Q^4	−109.8	−108.7	−109.8
Q^3	−101.1	−100.3	−100.3
Q^2	-	-	-
T^3	−65.3	−65.1	−66.6
T^2	-	−57.1	−58.5
T^1	-	-	−50.5

3.3. Sorption of Copper(II) and Nickel(II) Ions from Aqueous Solutions

The sorption studies of Cu(II) ions were carried out at pH ~5.5, and Ni(II) at ~6.5 [14], because the higher the pH, the better the sorption of these metals, but copper(II) and nickel(II) hydroxides begin to form at pH values ~5.5 and ~7, respectively [45]. As demonstrated in Figure 7, these materials are not an exception, and the best sorption of nickel(II) by all samples was observed at pH = 6. The addition of acids promotes the protonation of the amino groups reducing their sorption capacity. Meanwhile, the addition of alkali can cause the formation of basic metal salts. Therefore, aqueous solutions of salts with their natural pH were used in the sorption experiments.

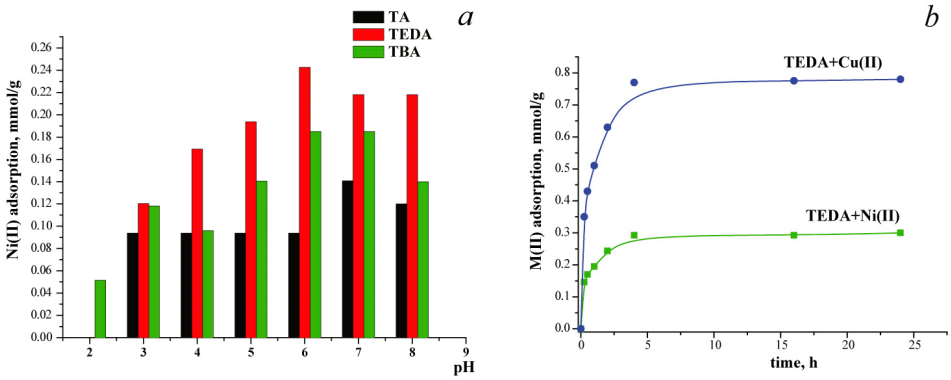

Figure 7. Dependence of nickel(II) ions adsorption on pH for all samples (**a**) and kinetic curves of Ni(II) (green line and symbols) and Cu(II) (blue line and symbols) sorption by **TEDA** sorbent (**b**).

The study of the kinetics of Ni^{2+} and Cu^{2+} sorption by the obtained sorbents was carried out in static mode. Graphically, the kinetics of the Ni^{2+} and Cu^{2+} sorption process by the **TEDA** sample (as an example) is presented in Figure 7. The kinetic curves of Ni(II) and Cu(II) sorption align well with the pseudo-second-order equation (Figure S3, Table S2): the cations sorption process occurs on the same type of active centres on the surface of functional silicas, but with the formation of different complexes. Although the initial uptake of Cu^{2+} by **TEDA** is faster than Ni^{2+}, the rate constant of Ni^{2+} sorption is higher. However, it appeared that 4 h of contact of **TEDA** with either of the mentioned ions was enough to establish a state of dynamic equilibrium. However, relying on our previous research [22,29], the establishment of adsorption equilibrium between copper cations and the samples with 3-aminopropyl groups lasted longer, so 24 h was chosen as the optimal time for further investigations of isothermal sorption.

The experimental isotherms of copper(II) and nickel(II) ions sorption on aminosilica particles, as well as their plots in the coordinates of the linearised Langmuir and Freundlich isotherm model equations, are illustrated in Figure 8, and Table 4 presents the parameters of Ni(II) and Cu(II) sorption. According to these calculations, the adsorption occurs on a heterogeneous surface for a **TA** sample with 3-aminopropyl groups, which are the simplest in structure among the others. This may be due to the fact that amino groups form hydrogen bonds with other amino and silanol groups [22], and adsorption occurs on adsorption centres of different energy. For the samples with diamine groups (**TEDA)** and secondary amines (**TBA)**, the isotherms are well fitted by the Langmuir model, which indicates chemisorption [46].

Moreover, the CLINP 2.1 program [47] was used to calculate the composition of the complexes formed on the surface of such sorbents. The composition of copper(II)/N-group complexes is 1/1 for the 3-aminopropyl group and 1/1 and 1/2 for the ethylenediamine and the secondary amine groups, respectively (Figure 8). In the case of nickel(II) complexes, their composition depends on the number of functional groups in the surface layer. If the group content is approximately 1 mmol/g, then complexes of composition 1/1 (**TA** sample) are formed, and if the group content increases, then 1/1 and 1/2 (for **TBA** sample) and 1/2 (for **TEDA** sample) complexes are formed. Thus, the number of nitrogen-containing groups and their structure determine the formation of various complexes on the surface, which affects the total sorption capacity of the samples.

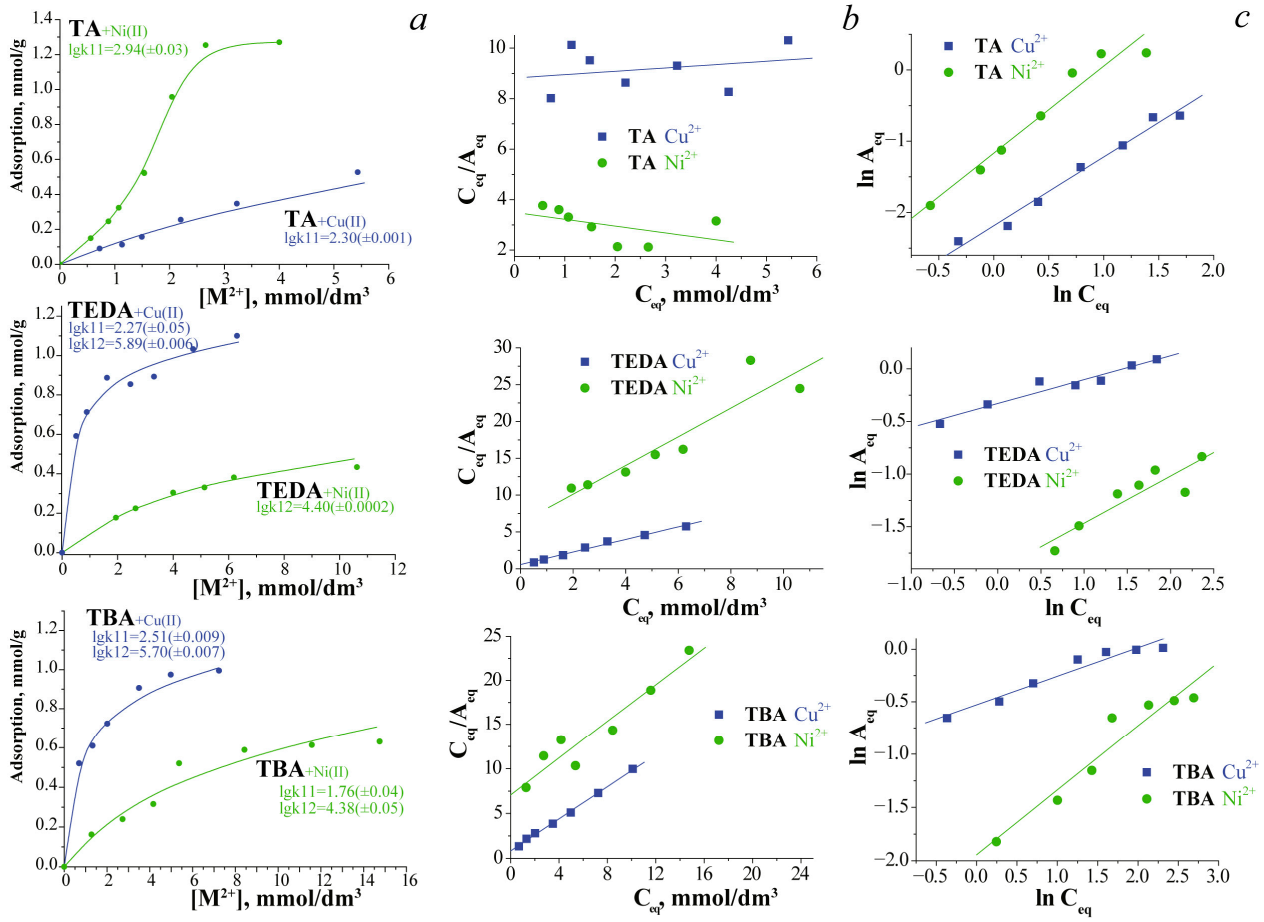

Figure 8. (**a**) Copper(II) and Nickel(II) adsorption isotherms (Adsorption vs. equilibrium concentration of metal ions [M^{2+}]) for amine-containing silica microspheres (points—experimental data, lines—calculated data); adsorption isotherms in the coordinates of the Langmuir (**b**) and Freundlich (**c**) equations.

Table 4. Parameters of Ni(II) and Cu(II) ions sorption in the Langmuir and Freundlich equations.

Sample	Cation	SSC, mmol/g	Langmuir Equation $C_{eq}/A_{eq} = 1/(K_L \cdot A_{max}) + (1/A_{max}) \cdot C_{eq}$			Freundlich Equation $\ln A_{eq} = \ln K_F + (1/n) \cdot \ln C_{eq}$		
			A_{max}, mmol/g	K_L, dm^3/mmol	R^2	K_F, mmol/g	n	R^2
TA	Ni(II)	1.27	−3.69	−0.077	0.2429	0.311	0.82	**0.9541**
	Cu(II)	0.53	7.54	0.015	0.0669	0.112	1.04	**0.9824**
TEDA	Ni(II)	0.43	0.51	0.314	**0.8599**	0.147	2.23	0.8206
	Cu(II)	1.09	1.17	1.512	**0.9888**	0.719	4.40	0.9397
TBA	Ni(II)	0.63	0.96	0.147	**0.9142**	0.143	1.65	**0.9274**
	Cu(II)	1.01	1.12	1.084	**0.9980**	0.589	3.68	0.9458

A_{eq}—adsorption capacity at equilibrium, mmol/g; K_L—the Langmuir constant, which characterises the adsorption energy, dm^3/mmol; C_{eq}—equilibrium concentration of metal ions in the solution, mmol/dm^3; A_{max}—maximal adsorption capacity for complete monolayer covering of the surface, mmol/g; K_F—a Freundlich constant, mmol/g; n—an empirical parameter related to the intensity of adsorption.

3.4. Albumin Adsorption Research

The adsorption of BSA on samples with different types of amino groups was also probed (Figure 9, Table 5). In terms of sorption capacity to BSA molecules, the tested samples can be

ranged as the following: **TBA** (204.6 mg/g) > **TEDA** (181.5 mg/g) > **TA** (78.3 mg/g). It was shown that such large protein molecules as BSA have a higher affinity to the materials with higher specific surface area and content of available amino groups for interactions, **TEDA** and **TBA**.

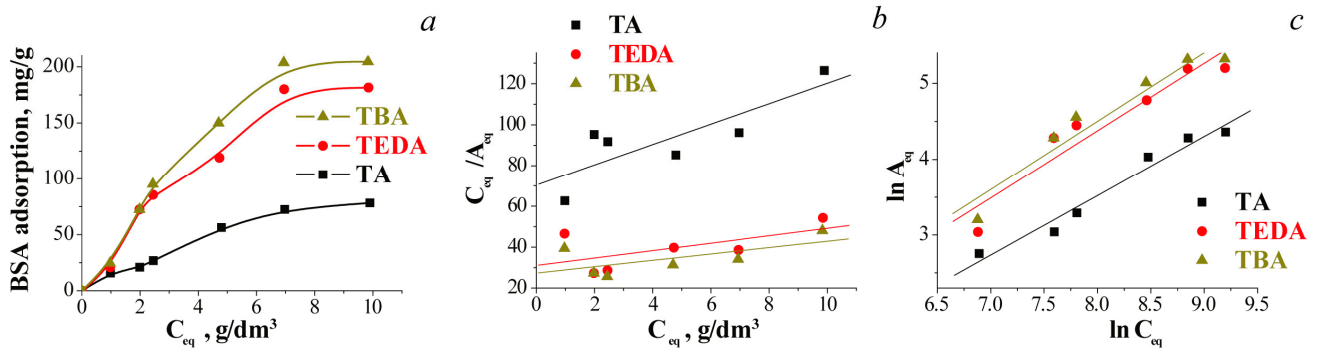

Figure 9. BSA adsorption isotherms for amine-containing silica microspheres (**a**); adsorption isotherms in the coordinates of the Langmuir (**b**) and Freundlich (**c**) equations.

Table 5. Parameters of BSA sorption in the Langmuir and Freundlich equations.

Sample	SSC, mg/g	Langmuir Equation $C_{eq}/A_{eq} = 1/(K_L \cdot A_{max}) + (1/A_{max}) \cdot C_{eq}$			Freundlich Equation $\ln A_{eq} = \ln K_F + (1/n) \cdot \ln C_{eq}$		
		A_{max}, mg/g	K_L, dm³/mg	R^2	K_F, mg/g	n	R^2
TA	78.3	200.8	0.0001	0.682	0.064	1.28	**0.965**
TEDA	181.5	549.5	0.0001	0.356	0.066	1.13	**0.904**
TBA	204.6	641.0	0.0001	0.400	0.067	1.11	**0.927**

A_{eq}—adsorption capacity at equilibrium, mmol/g; K_L—the Langmuir constant, which characterises the adsorption energy, dm³/mmol; C_{eq}—equilibrium concentration of metal ions in the solution, mmol/dm³; A_{max}—maximal adsorption capacity for complete monolayer covering of the surface, mmol/g; K_F—a Freundlich constant, mmol/g; n—an empirical parameter related to the intensity of adsorption.

The higher values of correlation coefficients of isotherms of BSA adsorption by all the studied samples with Freindlich isotherm model indicate adsorption on heterogeneous adsorption centres (Table 5). Thus, a **TBA** material, which apart from amino groups also contains the most significant among the samples hydrocarbon component, is characterised by the highest SSA value towards BSA. Moreover, the molecules of BSA can also be trapped between the aggregates of small particles of **TEDA** and **TBA** in the course of sorption.

4. Conclusions

The sol-gel method and its variant, Stöber technique, were applied for the synthesis of spherical silica particles containing 3-aminopropyl, ethylenediamine and secondary amine groups. It was demonstrated that the size of the obtained particles is affected by the size of the functional group (steric factor), the type of applied (methoxy or ethoxy) functionalising derivative, and, consequently, the hydrolysis rate, leading to the formation of spherical particles with 3-aminopropyl groups with a size up to 800 nm, and dendric silica particles with ethylenediamine and secondary amine groups making aggregates up to 275 nm. The presence of functional groups was qualitatively confirmed by IR spectroscopy, ^{13}C NMR spectroscopy, thermal analysis, and titration, and the quantitative content of functional groups available for interaction was 1.3–2.3 mmol/g. The calculated composition of surface complexes of metal ions indicates the complexation of one Cu(II) and Ni(II) ion with one or two surface amine-containing groups, depending on the concentration and geometry of the surface functional groups. Therefore, current research explains how under similar conditions of synthesis, functional silanes of a similar nature, but of a different structure, affect the morphology and the properties of the obtained materials. Using nitrogen-containing

silanes of various configurations, it is possible to form various complexes of copper(II) and nickel(II) on the surface, and to regulate the sorption capacity of the materials. Besides, the amino-containing spherical silicas are suitable for the adsorption of biomolecules, whereby the sorption activity of the samples depends on the number of available functional groups, the value of the specific surface and the presence of heterogeneous sorption centres on the surface.

Supplementary Materials: The following supporting information can be downloaded at: https://www.mdpi.com/article/10.3390/cryst13020190/s1, Figure S1: Pore-size distribution curves for the porous samples: TEDA and TBA plotted based on the SCV/SCR method; Figure S2: The EDXS spectra of the synthesised samples title; Figure S3: Kinetic curves of Ni(II) and Cu(II) sorption by **TEDA** silica in Lagergren equation coordinates for pseudo-first (left) and pseudo-second (right) order processes; Table S1: Structural and adsorption characteristics of the synthesised porous samples; Table S2: Kinetic parameters of Cu(II) and Ni(II) ions adsorption by the **TEDA** sample.

Author Contributions: Conceptualization, I.M.; Methodology, I.M., V.T. and N.S.; Software, I.M.; Formal analysis, V.T., N.S. and I.M.; Investigation, V.T., N.S. and I.M.; Resources, I.M.; Data curation, V.T., N.S. and I.M.; Writing-original draft preparation, N.S., V.T. and I.M.; Writing-review and editing, I.M.; Supervision, I.M.; Project administration, I.M. All authors have read and agreed to the published version of the manuscript.

Funding: The research was carried out within the Slovak Research and Development Agency (APVV-19-0302) and Ministry of Education, Science, Research and Sport of the Slovak Republic (VEGA 2/0116/23) projects.

Data Availability Statement: The data presented in this study are available on request from the corresponding author.

Conflicts of Interest: The authors declare no conflict of interest.

References

1. Briffa, J.; Sinagra, E.; Blundell, R. Heavy metal pollution in the environment and their toxicological effects on humans. *Heliyon* **2020**, *6*, e04691. [CrossRef] [PubMed]
2. Manahan, S.E. *Environmental Chemistry*, 7th ed.; Lewis Publishers: Boca Raton, FL, USA, 2000; p. 898.
3. Sharma, S.; Bhattacharya, A. Drinking water contamination and treatment techniques. *Appl. Water Sci.* **2017**, *7*, 1043–1067. [CrossRef]
4. Singh, B.; Na, J.; Konarova, M.; Wakihara, T.; Yamauchi, Y.; Salomon, C.; Gawande, M.B. Functional mesoporous silica nanomaterials for catalysis and environmental applications. *Bull. Chem. Soc. Jpn.* **2020**, *93*, 1412–1608. [CrossRef]
5. Gomes, A.L.M.; Andrade, P.H.M.; Palhares, H.G.; Dumont, M.R.; Soares, D.C.F.; Volkringer, C.; Houmard, M.; Nunes, E.H.M. Facile sol-gel synthesis of silica sorbents for the removal of organic pollutants from aqueous media. *J. Mater. Res. Technol.* **2021**, *15*, 4580–4594. [CrossRef]
6. Pietras-Ożga, D.; Piątkowska-Sawczuk, K.; Duro, G.; Pawlak, B.; Stolyarchuk, N.; Tomina, V.; Melnyk, I.; Giannakoudakis, D.A.; Barczak, M. Chapter 9-Sol-gel–derived silica xerogels: Synthesis, properties, and their applicability for removal of hazardous pollutants. In *Advanced Materials for Sustainable Environmental Remediation*; Giannakoudakis, D., Meili, L., Anastopoulos, I., Eds.; Elsevier: Amsterdam, The Netherlands, 2022; pp. 261–277; ISBN 9780323904858. [CrossRef]
7. Sarker, M.Z.; Rahman, M.M.; Minami, H.; Suzuki, T.; Ahmad, H. Amine functional silica–supported bimetallic Cu-Ni nanocatalyst and investigation of some typical reductions of aromatic nitro-substituents. *Colloid Polym. Sci.* **2022**, *300*, 279–296. [CrossRef]
8. Tomina, V.V.; Furtat, I.M.; Stolyarchuk, N.V.; Zub, Y.L.; Kanuchova, M.; Vaclavikova, M.; Melnyk, I.V. Surface and structure design of aminosilica nanoparticles for multifunctional applications: Adsorption and antimicrobial studies. In *Micro and Nano Technologies, Biocompatible Hybrid Oxide Nanoparticles for Human Health*; Melnyk, I.V., Vaclavikova, M., Seisenbaeva, G.A., Kessler, V.G., Eds.; Elsevier: Amsterdam, The Netherlands, 2019; pp. 15–31. ISBN 9780128158753. [CrossRef]
9. Miller, P.J.; Shantz, D.F. Covalently functionalized uniform amino-silica nanoparticles. Synthesis and validation of amine group accessibility and stability. *Nanoscale Adv.* **2020**, *2*, 860. [CrossRef]
10. Cuoq, F.; Masion, A.; Labille, J.; Rose, J.; Ziarelli, F.; Prelot, B.; Bottero, J.-Y. Preparation of amino-functionalized silica in aqueous conditions. *Appl. Surf. Sci.* **2013**, *266*, 155–160. [CrossRef]
11. Amino-Functionalized Silica Gel Spherical. Available online: https://www.sigmaaldrich.com/UA/en/product/supelco/79297?gclid=CjwKCAiAnZCdBhBmEiwA8nDQxY8ctBH_7HW0TXpTAb5pzwWL7WszPYaDBmX3zYJPAQ0s61SM9cd8hoC_K0QAvD_BwE&gclsrc=aw.ds (accessed on 30 December 2022).
12. Amine Functionalized Silica Nanoparticles. Available online: https://www.geandr.com/products/amine-functionalized-silica-nanoparticles (accessed on 30 December 2022).

13. Stöber, W.; Fink, A.; Bohn, E. Controlled growth of monodisperse silica spheres in the micron size range. *J. Colloid Interface Sci.* **1968**, *26*, 62–69. [CrossRef]
14. He, Y.; Luo, L.; Liang, S.; Long, M.; Xu, H. Amino-functionalized mesoporous silica nanoparticles as efficient carriers for anticancer drug delivery. *J. Biomater. Appl.* **2017**, *32*, 524–532. [CrossRef]
15. Martínez-Carmona, M.; Ho, Q.P.; Morand, J.; García, A.; Ortega, E.; Erthal, L.C.S.; Ruiz-Hernandez, E.; Santana, M.D.; Ruiz, J.; Vallet-Regí, M.; et al. Amino-functionalized mesoporous silica nanoparticle-encapsulated octahedral organoruthenium complex as an efficient platform for combatting cancer. *Inorg. Chem.* **2020**, *59*, 10275–10284. [CrossRef]
16. Kardys, A.Y.; Bharali, D.J.; Mousa, S.A. Amino-functionalized silica nanoparticles: In vitro evaluation for targeted delivery and therapy of pancreatic cancer. *J. Nanotechnol.* **2013**, *2013*, 768724. [CrossRef]
17. Tomina, V.; Furtat, I.; Lebed, A.; Kotsyuda, S.; Kolev, H.; Kanuchova, M.; Marcin Behunova, D.; Vaclavikova, V.; Melnyk, I. Diverse pathway to obtain antibacterial and antifungal agents based on silica particles functionalized by amino and phenyl groups with Cu(II) ions complexes. *ACS Omega* **2020**, *5*, 15290–15300. [CrossRef] [PubMed]
18. Liu, H.; Guo, Y.; Wang, X.; Liang, X.; Liu, X.; Jiang, S. A novel fullerene oxide functionalized silica composite as stationary phase for high performance liquid chromatography. *RSC Adv.* **2014**, *4*, 17541–17548. [CrossRef]
19. Gao, J.; Wu, S.; Tan, F.; Tian, H.; Liu, J.; Lu, G.Q.M. Nanoengineering of amino-functionalized mesoporous silica nanospheres as nanoreactors. *Progress in Natural Science: Mater. Int.* **2018**, *28*, 242–245. [CrossRef]
20. Cheedarala, R.V.; Chalapathi, K.V.; Song, J.I. Delayed flammability for natural fabrics by deposition of silica core-amine shell microspheres through dip-coating process. *Chem. Eng. J. Adv.* **2021**, *8*, 100164. [CrossRef]
21. Attia, M.F.; Anton, N.; Bouchaala, R.; Didier, P.; Arntz, Y.; Messaddeq, N.; Klymchenko, A.S.; Mely, Y.; Vandamme, T.F. Functionalization of nano-emulsions with an amino-silica shell at the oil–water interface. *RSC Adv.* **2015**, *5*, 74353–74361. [CrossRef]
22. Melnyk, I.V.; Tomina, V.V.; Stolyarchuk, N.V.; Seisenbaeva, G.A.; Kessler, V.G. Organic dyes (acid red, fluorescein, methylene blue) and copper(II) adsorption on amino silica spherical particles with tailored surface hydrophobicity and porosity. *J. Mol. Liq.* **2021**, *336*, 116301. [CrossRef]
23. Peng, S.; Deng, Y.; Li, W.; Chen, J.; Liuac, H.; Chen, Y. Aminated mesoporous silica nanoparticles for the removal of low-concentration malodorous aldehyde gases. *Environ. Sci. Nano* **2018**, *5*, 2663–2671. [CrossRef]
24. Hamdy, L.B.; Goel, C.; Rudd, J.A.; Barron, A.R.; Andreoli, E. The application of amine-based materials for carbon capture and utilisation: An overarching view. *Mater. Adv.* **2021**, *2*, 5843–5880. [CrossRef]
25. Howard, A.G.; Khdary, N.H. Nanoscavenger based dispersion preconcentration; sub-micron particulate extractants for analyte collection and enrichment. *Analyst* **2005**, *130*, 1432–1438. [CrossRef]
26. Li, J.; Miao, X.; Hao, Y.; Zhao, J.; Sun, X.; Wang, L. Synthesis, amino-functionalization of mesoporous silica and its adsorption of Cr(VI). *J. Colloid Interface Sci.* **2008**, *318*, 309–314. [CrossRef] [PubMed]
27. Dobrowolski, R.; Oszust-Cieniuch, M.; Dobrzyńska, J.; Barczak, M. Amino-functionalized SBA-15 mesoporous silicas as sorbents of platinum (IV) ions. *Colloids Surf. A: Physicochem. Eng. Asp.* **2013**, *435*, 63–70. [CrossRef]
28. Melnyk, I.V. Aminosilica nano-and submicrospheres: Study of influence factors on morphology, structure and properties. *Chem. J. Mold.* **2014**, *9*, 123–127. [CrossRef] [PubMed]
29. Tomina, V.; Melnyk, I.; Zub, Y.; Kareiva, A.; Vaclavikova, M.; Seisenbaeva, M.; Kessler, V. Tailoring bifunctional hybrid organic-inorganic nanoadsorbents by the choice of functional layer composition probed by adsorption of Cu^{2+} ions. *Beilstein J. Nanotechnol.* **2017**, *8*, 334–347. [CrossRef] [PubMed]
30. Akdemir, E.; Imamoglu, M. Solid-phase extraction of trace Ni(II) ions on ethylenediamine-silica material synthesized by sol–gel method. *Desalination Water Treat.* **2013**, *52*, 4889–4894. [CrossRef]
31. Khdary, N.H.; Ghanem, M.A. Metal–organic–silica nanocomposites: Copper, silver nanoparticles–ethylenediamine–silica gel and their CO_2 adsorption behaviour. *J. Mater. Chem.* **2012**, *22*, 12032–12038. [CrossRef]
32. Randall, J.P.; Meador, M.A.B.; Jana, S.C. Polymer reinforced silica aerogels: Effects of dimethyldiethoxysilane and bis(trimethoxysilylpropyl)amine as silane precursors. *J. Mater. Chem. A* **2013**, *1*, 6642–6652. [CrossRef]
33. Haghighat, M.; Shirini, F.; Golshekan, M. Periodic mesoporous organosilica containing bridges with N-sulfonic acid groups: A new catalyst for the efficient formylation of amines and alcohols. *Silicon* **2020**, *12*, 2087–2098. [CrossRef]
34. Khatib, I.S.; Parish, R.V. Insoluble ligands and their application. I. A comparison of silica-immobilized ligands and functionalized polysiloxanes. *J. Organomet. Chem.* **1989**, *369*, 9–16. [CrossRef]
35. Brunauer, J.S.; Emmet, P.H.; Teller, E. Adsorption of gases in multimolecular layers. *J. Am. Chem. Soc.* **1938**, *60*, 309–319. [CrossRef]
36. Brinker, C.J. Hydrolysis and condensation of silicates: Effects on structure. *J. Non-Cryst. Solids* **1988**, *100*, 31–50. [CrossRef]
37. Brinker, C.J.; Scherer, G.W. *The Physics and Chemistry of Sol-Gel Processing*; Academic Press: Cambridge, MA, USA, 1990; p. 908. ISBN 978-0-08-057103-4. [CrossRef]
38. Gun'ko, V.M. Composite materials: Textural characteristics. *Appl. Surf. Sci.* **2014**, *307*, 444–454. [CrossRef]
39. Colthup, N.B.; Daly, L.H.; Wiberley, S.E. Amines, C=N, And N=O Compounds. In *Introduction to Infrared and Raman Spectroscopy*; Academic Press: Cambridge, MA, USA, 1990; pp. 339–354. [CrossRef]
40. Rymuszka, D.; Terpiłowski, K.; Sternik, D.; Tomczyńska-Mleko, M.; Goncharuk, O. Wettability and thermal analysis of hydrophobic poly(methyl methacrylate)/silica nanocomposites. *Adsorpt. Sci. Technol.* **2017**, *35*, 560–571. [CrossRef]

41. Zub, Y.L.; Melnyk, I.V.; Stolyarchuk, N.V.; Dobryanska, H.I.; Barczak, M.; Dabrowski, A. Comparative characteristics of texture and properties of hybrid organic–inorganic adsorbents functionalized by amine and thiol groups. *Prog. Solid State Chem.* **2005**, *33*, 179–186. [CrossRef]
42. Ostwal, M.; Singh, R.P.; Dec, S.F.; Lusk, M.T.; Way, J.D. 3-Aminopropyltriethoxysilane functionalized inorganic membranes for high temperature CO_2/N_2 separation. *J. Membr. Sci.* **2011**, *369*, 139–147. [CrossRef]
43. Wahab, M.A.; Kim, I.; Ha, C.-K. Bridged amine-functionalized mesoporous organosilica materials from 1,2-bis(triethoxysilyl)ethane and bis[(3-trimethoxysilyl)propyl]amine. *J. Solid State Chem.* **2004**, *177*, 3439–3447. [CrossRef]
44. Park, K.-W.; Jeong, S.-Y.; Kwon, O.-Y. Interlamellar silylation of H-kenyaite with 3-aminopropyltriethoxysilane. *Appl. Clay Sci.* **2004**, *27*, 21–27. [CrossRef]
45. Stolyarchuk, N.; Tomina, V.; Biswajit, M.; Tripathi, B.P.; Václavíková, M.; Dudarko, O.; Melnyk, I. Direct synthesis of efficient silica-based adsorbents carrying EDTA groups for the separation of Cu(II) and Ni(II) ion. *Colloids Surf. A: Physicochem. Eng. Asp.* **2022**, *650*, 129538. [CrossRef]
46. Tomina, V.; Stolyarchuk, N.; Semeshko, O.; Barczak, M.; Melnyk, I. Diamine groups on the surface of silica particles as complex-forming linkers for metal cations. *Molecules* **2023**, *28*, 430. [CrossRef]
47. CLINP 2.1, a Software Program for Computation of Stability Constants and Physicochemical Parameters of Complex Compounds in Solutions, Extractional and Sorptional Systems on the Base of Composition-Property Dependencies. Available online: http://chemo.univer.kharkov.ua/kholin/clinp.html (accessed on 30 December 2022).